EasyChair Preprint

№ 10350

Characterization of Slag-Based Mix Activated with Hydrated Lime of Industrial Grade: a Short Communication

Jayashree Sengupta and Nirjhar Dhang

November 29, 2023

Characterization of Slag-based mix Activated with Hydrated Lime of Industrial Grade: A Short Communication

Jayashree Sengupta[1], Nirjhar Dhang[2]

[1]Research Scholar, Dept. of Civil Engineering, Indian Institute of Technology, Kharagpur, West Bengal 721302, India (corresponding author). ORCID: https://orcid.org/0000-0002-6892-3480.
Email: jaish.sengupta@iitkgp.ac.in

[2]Professor, Dept. of Civil Engineering, Indian Institute of Technology, Kharagpur, West Bengal 721302, India.
Email: nirjhar@civil.iitkgp.ac.in

Abstract

The objective of this study is to examine whether industrial-grade hydrated lime can serve as an effective alkali activator in a one-part system. While previous experiments have showcased the positive impact of introducing calcium in alkali-activated concrete, the current investigation reveals that relying solely on hydrated lime did not yield a significant improvement in strength. Additionally, surpassing a hydrated lime content of 30% had adverse effects, leading to a notable decline in strength. Microstructural analysis demonstrated a prevalence of CSH gel over CASH polymeric gel, indicating that pozzolanic reactions took precedence over the polymerization process, resulting in the production of concrete with low-to-medium strength.

Keywords

Lime-activated slag mortar, ground-granulated blast furnace slag, alkali activation, microstructure

1. Introduction

There is a pressing need for raw building materials that are both environmentally and technically sound alternatives to standard cementitious concrete. The production of concrete and commonly used construction materials involves significant energy consumption and CO_2 emissions. Despite concrete maintaining its status as the primary building material, there is a growing need for more eco-friendly alternatives. Alkali-activated concretes play a crucial role by recycling industrial waste into aluminosilicate precursors, which exhibit binding properties when activated by alkalis.

This process involves the complete replacement of cement and reportedly results in improved mechanical properties compared to Ordinary Portland Cement (OPC). However, the widespread application of alkali-activated concrete is hindered by the handling of toxic alkali solutions and the need for skilled labor in in-situ castings. To address these challenges, alkali-activated mixes are categorized into two-part mixes and one-part mixes. The latter involves a dry mixture of solid activators, additives, and precursors pre-blended to form a single binder, following a "just-add-water" approach similar to conventional concreting. Consequently, one-part geopolymer mixes contribute to sustainable concrete practices by reducing cement usage, recycling industrial by-products like slag and fly ash as precursors, and facilitating user-friendly in-situ casting without caustic solutions.

In the case of two-part geopolymers, precursor materials undergo activation through highly caustic alkaline solutions, with these activators altering the mix's pH and initiating the dissolution process. Activators can be basic or acidic, with common alkali family activators (Na+, K+) and alkali earth activators (Ca^{+2}, Mg^{+2}). Acidic activators include H3PO4 [1]–[4] and citric acid [5], though hydrates may not be stable products [6]. Even in one-part geopolymers, alkali particles dissolve, releasing hydroxyl ions that elevate the system's pH, leading to network formation with the release of silica and alumina. Over time, the pH decreases with OH^- ion intake, catalyzing ion exchange during the hydrolysis-deprotonation of susceptible Si-O-Si bonds in the aluminosilicate precursor. Weaker Si-O-Si bonds dissolve faster at pH >11, while Al-O bonds dissolve faster at pH >6. The addition of calcium results in a stable 3D framework at pH <12 [7]. The presence of calcium-rich phases positively influences mechanical strength by forming distinct phases of CSH and polymeric gel, bridging and densifying the microstructure [8]. Hydroxyl groups and divalent calcium ions react to form a precipitate, raising the pH and providing sites for silicate polymerization and nucleation [9]. The continuous formation of binding gels (CSH, CASH, NCASH) depends on the availability of calcium ions and the mixture's pH. Adequate calcium ions are crucial for promoting the reaction between silicate and aluminate tetrahedrons [10]. Calcium ion addition to precursors, such as clay from the brick industry [11], has proven favorable for improving mechanical properties. Nevertheless, it has been reported [12]that dissolution is delayed, along with the formation of oligomers, due to competition between alkali cations Ca^{+2} and Na^+ for Lewis acidity. The use of hydrated lime as a solid activator thus presents an intriguing area for study, besides the usual highly reactive alkali solutions.

Before the advent of cement, hydraulic lime served as an excellent building material. The literature highlights the strength and durability properties of lime-pozzolana mixes [13], [14], with ancient Greeks and Romans appreciating the combination of lime mortars with reactive aluminosilicates [15], [16]. Lime not only functioned as a building material but also as an alkali activator. The strengthening of Roman concrete over time was attributed to the precipitation of phillipsite and Al-tobermorite crystals through reactions with seawater and ionic exchanges with pozzolanic alkaline aggregates and seawater, setting the foundation for geopolymers as termed by Davidovits [17], [18]. The pozzolanic reactivity and curing conditions significantly influenced the carbonation reaction in the hydration process of typical lime-pozzolanic blends[19]. Moist regimes were crucial for ensuring adequate strength during hydration, as dry regimes led to slowed or halted reactions due to full carbonation of lime. Addressing the carbonation degree in high calcium mixes became a critical concern. In a study[20], the addition of nano-silica and nano-alumina to lime-pozzolana blends demonstrated promising results. Nano-silica reduced porosity and carbonation values while enhancing compressive strength, resulting in a densified microstructure [21]. This suggests that the incorporation of silica, particularly when activated by hydrated lime, could offer benefits.

These findings prompt a shift towards understanding the characteristics of reactive aluminosilicate binders and the resulting alterations in the properties of the mix. An in-depth exploration of specific by-products was conducted to elucidate their advantages and lingering uncertainties [22]. Alkali-activated binders, recognized as the "epicenter" of cement technology, were extensively reviewed [23] for their potential and scope. Industrial by-products exhibiting pozzolanic properties emerged as suitable aluminosilicate precursors for geopolymers and have been a focal point of research [22], [24]–[26] in recent decades. Comprehensive analyses by Luukkonen et al. [27] delved into the merits and drawbacks of one-part alkali-activated binders, highlighting their potential as environmentally friendly components for concrete production. While such concrete displayed lower strength due to increased crystalline zeolitic formation, the addition of silica fume and red mud [28] yielded promising strength outcomes. In alkali-activated mixes, the amorphous gel strengthened the interfacial transition zone, countering the typical weakening effect of portlandite crystallinity [29] in cement microstructures. Regulating water content in one-part geopolymers prevented crystalline microstructure formation [30]. The presence of rice husk ash enhanced strength through the hydration of the CaO content in GGBFS, forming additional CSH gel and densifying the matrix [31]. Silica fume-treated alkali-activated red mud dissolved to create

geopolymer micelles [28], coexisting with CSH and densifying the microstructure. Increased alkali concentration further improved the pore structure [32].

Past studies have emphasized the efficacy of analytical-grade chemicals in activating aluminosilicates, given their high reactivity at 99% purity. Despite their efficiency, these chemicals are costly. Addressing this limitation, using industrial grade hydrated lime as a solid activator to activate ground granulated blast furnace slag (GGBFS) with silica fume (SF) as an additive seemed unprecedented and exploratory. The same is thus investigated in this brief communication, varying percentages of hydrated lime and SF, ranging up to 40%

2. Experimental Methods

The aluminosilicate precursor employed in this investigation was ground granulated blast furnace slag (GGBFS), sourced from Rashmi Cement Limited in West Bengal, India. Hydrated lime powder for industrial use was locally procured from Shreeram Chemicals, while silica fume (SF) was obtained from Waltar Enterprises. Figure 1 illustrates the XRD spectra of the precursors and solid activator. Table 1 provides information on the physical characteristics and chemical compositions of the precursor and additive. It is essential for the slag to be neutral or basic for alkali activation, and the slag used in this study met these requirements, with a basicity (B) of 1.14 and CaO/SiO_2 ratio of 1.36.

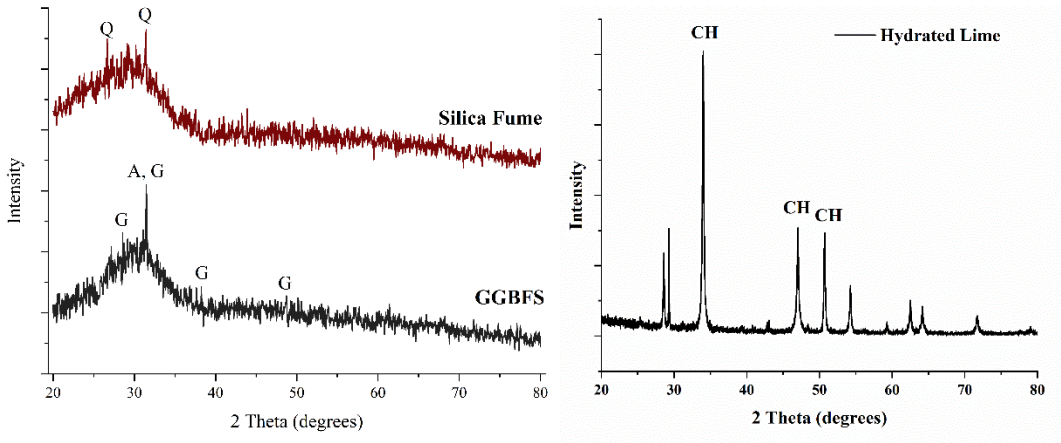

Figure 1: XRD images of the raw materials GGBFS, Silica fume, and Hydrated lime. Q: Quartz, A: Akermenite, G: Gehlenite, CH: Calcium hydroxide

Table 1: Chemical and physical properties of the raw materials

	Chemical Properties											Physical Properties		
	CaO	SiO_2	Al_2O_3	MgO	MnO	K_2O	Na_2O	Fe_2O_3	TiO_2	P_2O_5	SO^3	Appearance	Density (kg/m^3)	Blaine Fineness (m^2/kg)
GGBS	43.78	32.08	11.20	5.82	0.84	0.42	0.03	0.75	0.87	1.33	1.65	Greyish White	2890	385
SF	3.81	84.12	0.15	1.43	1.15	2.70	0.02	2.64	0.40	0.72	0.33	Greyish Black	2170	589

Table 2 displays the distinct groups of mortar samples, formed by altering the percentages of silica fume and hydrated lime. Both hydrated lime and silica fume were varied up to a 40% addition as a replacement percentage of GGBFS. The table presents the mix proportions and molar ratios, labeled accordingly. The designations L and SF indicate the percentages of hydrated lime and silica fume, respectively, with the associated number representing the percentage. In all mixes, the water/binder ratio is maintained at 0.45, while the aggregate/binder ratio is kept constant at 3.0 for casting the mortar samples.

Table 2: Weight fractions of the mix blends using hydrated lime as a solid activator to activate GGBFS with silica fume (SF) as an additive. The variations in the molar ratio are also calculated. The w/b is taken as 0.45 and the aggregate/binder is taken as 3.0.

MIX ID	Wt. fraction of the binder			SiO_2/Al_2O_3	CaO/SiO_2	H_2O/CaO
	GGBS	SF	SL			
L10SF10	0.80	0.10	0.10	6.408	1.34	3.284
L10SF20	0.70	0.20	0.10	8.407	1.05	3.62
L10SF30	0.60	0.30	0.10	11.050	0.83	4.041
L10SF40	0.50	0.40	0.10	14.710	0.66	4.567
L20SF10	0.70	0.10	0.20	6.585	1.57	3.075
L20SF20	0.60	0.20	0.20	8.911	1.23	3.37
L20SF30	0.50	0.30	0.20	12.119	0.97	3.729
L20SF40	0.40	0.40	0.20	16.831	0.77	4.173
L30SF10	0.60	0.10	0.30	6.815	1.85	2.891
L30SF20	0.50	0.20	0.30	9.592	1.43	3.15
L30SF30	0.40	0.30	0.30	13.649	1.13	3.462
L30SF40	0.30	0.40	0.30	20.142	0.89	3.841
L40SF10	0.50	0.10	0.40	7.125	2.20	2.728
L40SF20	0.40	0.20	0.40	10.562	1.68	2.96
L40SF30	0.30	0.30	0.40	16.022	1.31	3.231
L40SF40	0.20	0.40	0.40	26.034	1.04	3.558

For thorough mixing, GGBFS, silica fume, and hydrated lime were combined in a pan and dry-mixed for approximately one minute. Subsequently, the standard sand mixture was introduced to the dry blend, followed by the addition of tap water. Each mixing sample was cast in 70.6 mm cubes, arranged in two sets of triplets, and compacted for 2 minutes in a vibrating machine. Compressive strengths of the mortar triplets were evaluated after curing for 7 and 28 days at room temperature and 100% RH. SEM images were obtained to examine the microstructure of the activated mortar samples. Powdered mortar pieces were collected after compressive strength testing. These samples underwent a 45-minute exposure to acetone, followed by 5 minutes of air drying. After air drying, a two-hour, 60°C oven drying process was applied. The samples were then kept in a vacuum desiccator until testing for SEM and XRD. From each group, especially up to 30% of lime addition, the hardened samples with the highest compressive strength were selected. Microstructural images were analyzed using a FEGSEM (field emission-gun scanning electron microscope), specifically the ZEISS Merlin Scanning Electron Microscope. The acceleration voltage used for all analyses varied between 5-15 kV as per requirements, and the samples were gold-coated before testing to ensure precise measurements.

3. Results and Discussions

When water was introduced to the mix, $Ca(OH)_2$ underwent hydrolysis, breaking down into Ca^{+2} and OH^-. The presence of OH^- triggered the dissociation of slag particles by breaking Si-O, Al-O, and Ca-O bonds, resulting in the formation of Ca^{+2}, Al^{+3}, $Si(OH)^{-4}$, and $Al(OH)^{-4}$. Through polycondensation, $Si(OH)^{-4}$, and $Al(OH)^{-4}$ generated dimers of Si-O-Si and Al-O-Al, eventually leading to the formation of C-A-S-H gels. However, with the addition of more hydrated lime to the system, the calcium concentration increased. Colloidal $Ca(OH)_2$ was also formed as part of the ongoing process. This, in conjunction with $[SiO_3]^{-2}$ from silica fume, led to the generation of additional C-S-H gels. Consequently, the coexistence of the two gels (CASH and CSH) contributed to the strength of the mix. Nevertheless, varying the proportions of hydrated lime and silica fume did not significantly alter the strength, as depicted in figure 2. The 28-day strength ranged from 20.53 to 27.16 MPa. However, silica fume content exceeding 30% in each set of lime substitution proved unfavorable. Moreover, according to Figure 2, it is evident that the optimal percentage for silica fume was apparently 20%, beyond which there was a reduction in strength. As no systematic variation in the strength was evident, the strength variations were delved into the according to molar ratios, as shown in Table 2. A scattered plot was observed, and the best fit

of the variation is illustrated in figure 3. Both 7-day and 28-day strength decreased with an increased H_2O/CaO ratio, attributed to the dilution effect by increased OH^-. However, since GGBFS was not the sole provider of Ca^{+2} ions, higher CaO indicated increased possibilities of colloidal $Ca(OH)_2$ formation. Consequently, more CSH would form as a secondary reaction product, explaining the larger slope for 28-day strength development in figure 5. SEM images also revealed $Ca(OH)_2$ crystal production after 7 days of curing. Compressive strength increased with an increased CaO/SiO_2 ratio, as indicated in the figure. As Al_2O_3 generally serves as a network constructor, an increased SiO_2/Al_2O_3 ratio suggested reduced Al_2O_3 availability for polymer network development. This, in turn, could diminish the likelihood of C-A-S-H production and result in a drop in strength.

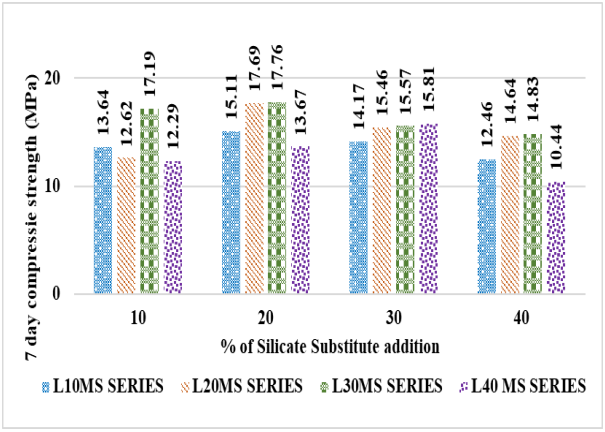

(a)

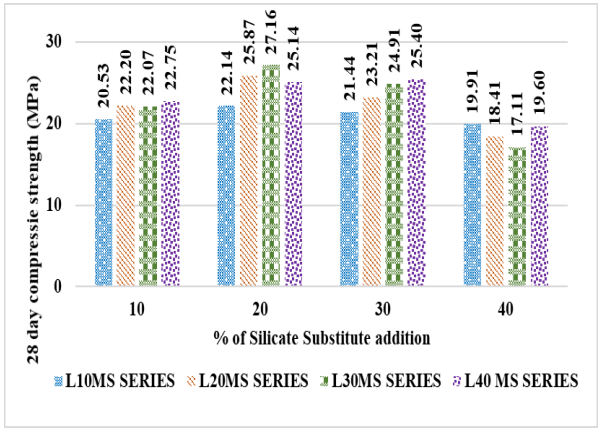

(b)

Figure 2: 7-day and 28-day strength development of the mix blended with SF and activated with hydrated lime (L) with the % variation in the silica fume addition

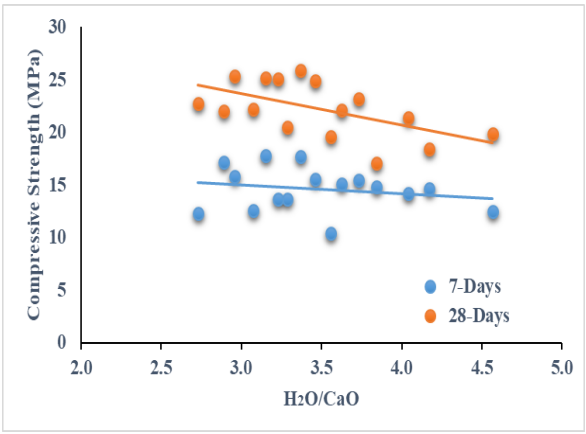

(a)

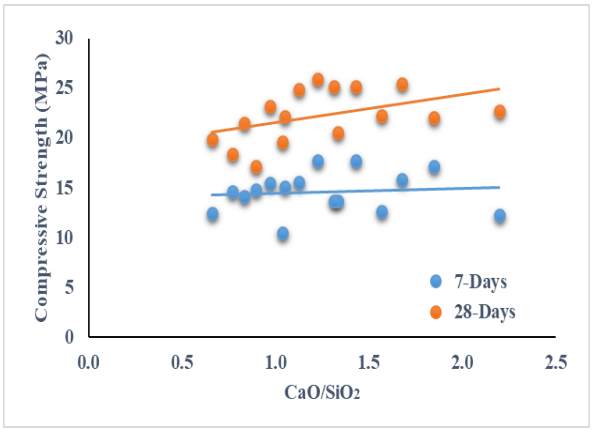

(b)

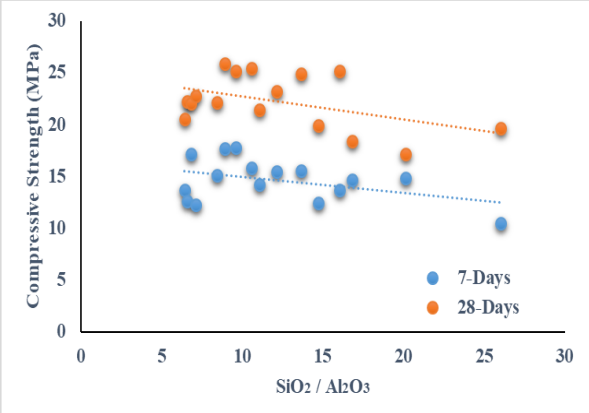

(c)

Figure 3: Variation of the compressive strength with the molar ratios

Figure 4 illustrates the XRD results of the samples, selected based on the maximum strength in each set up to 30% silica fume. The data for the 40% hydrated lime, which exhibited lower maximum strength compared to the 30% hydrated lime, is not included in the figure. The XRD analysis revealed calcite (98-011-0799) as the major peak at 29.3, 36.1, 39.5, 43.1 and 48.4 (2θ°), with a prominent brucite (98-002-1508) peak at 39.9 (2θ°) and a minor portlandite (98-005-3829) peak at 36.1 (2θ°). While no significant peaks were observed, minor peaks of thaumasite (98-001-2249) and ettringite (98-000-5652) were present, indicating the presence of AFt and AFm phases, similar to cement hydration. These crystalline phases, known to weaken the microstructure [29], explained the medium strength development in the samples. Controlling the water content was suggested as a means to prevent the formation of the crystalline microstructure [30]. Additionally, magnesite (98-002-1915) exhibited peaks at 32.8 and 43.27 (2θ°), and dolomite (98-006-2971) peaks were apparent at 35.6 (2θ°). A noticeable convex hump in the XRD analysis, occurring between 26 (2θ°) and 35 (2θ°), indicated the presence of C-S-H gel, specifically in the form of Tobermorite 14A (98-010-4719). The degree of convexity in the hump correlated with higher gel formation. C-A-S-H, represented by Zeolite X (Ca-exchanged, 98-002-8671), was also observed. Rietveld analysis of the XRD graphs (as shown in Table 3) further confirmed that the microstructure was rich in C-S-H and calcite morphologies, with less pronounced polymeric C-A-S-H. Table 3 indicates that L30SF20 exhibited a higher presence of hydrotalcite, along with CSH and CASH, contributing to the strength development of the sample. The addition of MgO to GGBFS blends has been reported to enhance mechanical strength by promoting hydrotalcite formation [33], [34]. This explains why L30SF20 achieved a maximum strength of 27.16 MPa.

Table 3: Percentages of phases as analysed by Rietveld analysis in Xpert Highscore 3 software.

Phases	L10SF20	L20SF20	L30SF20
Calcite	33.8	37.8	34.4
Magnesite	7.4	4.5	0
Dolomite	2.9	3.6	1.3
Portlandite	1.7	3.3	1.1
Brucite	6.8	7.4	6.9
Hydrotalcite	0	0	2.1
Thaumasite	5.9	5	6.4
Ettringite	1.9	1.3	3.8
Tobermorite 14A	34.4	29.3	34.7
Zeolite X	5.2	8.8	9.2

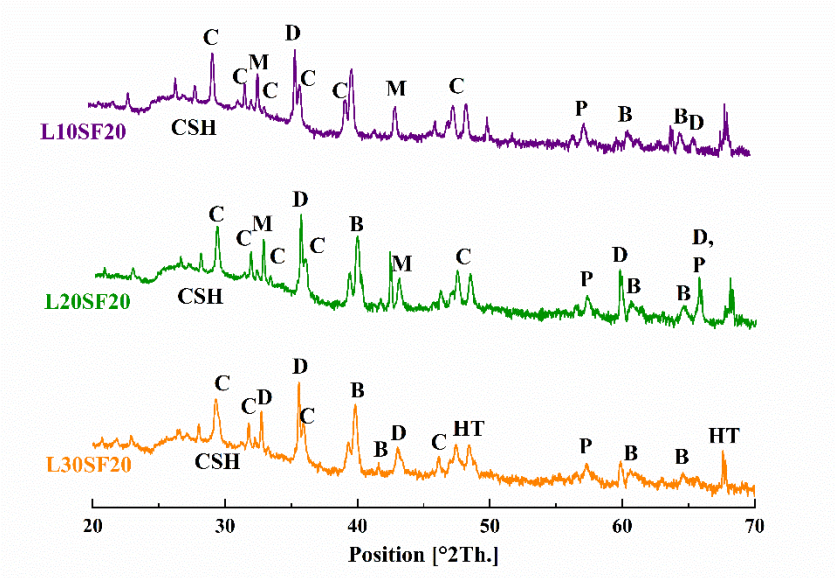

Figure 4: XRD images of L10SF20, L20SF20, and L30SF20 mortar at 28 days. C: Calcite, P: Portlandite, B: Brucite, M: Magnesite, D: Dolomite, HT: Hydrotalcite, CSH: Calcium silicate hydrate gel

Figures 5–7 display SEM images for L10SF20, L20SF20, and L30SF20. The microstructure was rich in fibrous C-S-H morphologies rather than scaled morphologies of C-A-S-H formation. Thin hexagonal plate-like formations, characteristic of portlandite, were also evident in the majority of the 7-day samples. Notably, L30SF20 exhibited typical double-layered morphologies indicative of hydrotalcite. These double-layered calcium magnesium hydroxides, known to contribute to strength gain, help explain why L30SF20 demonstrated the highest strength among the various mixes.

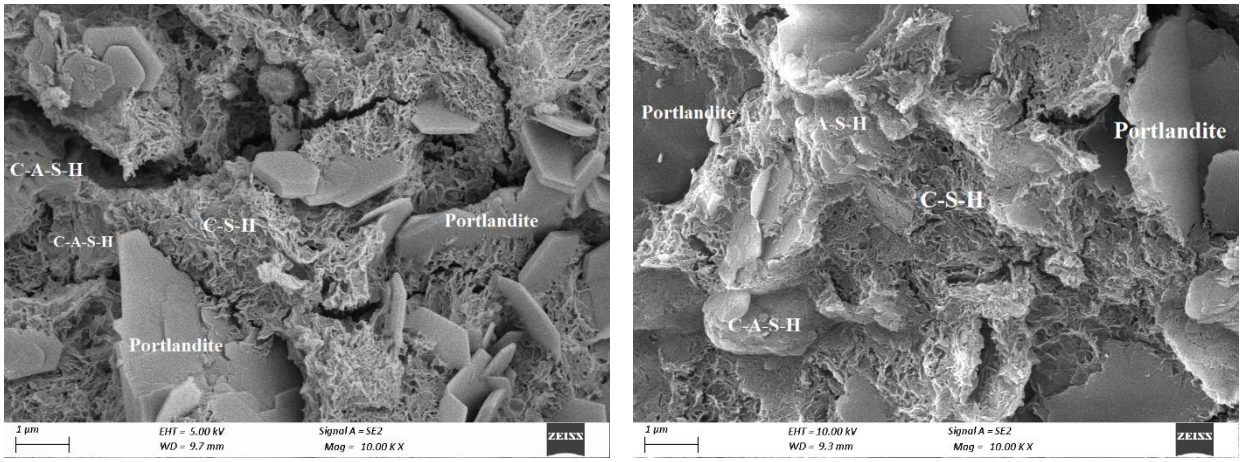

(a) (b)

Figure 5: SEM images of L10SF20 mortar containing 20% hydrated lime and 20% silica fume at (a) 7 days (b) 28 days

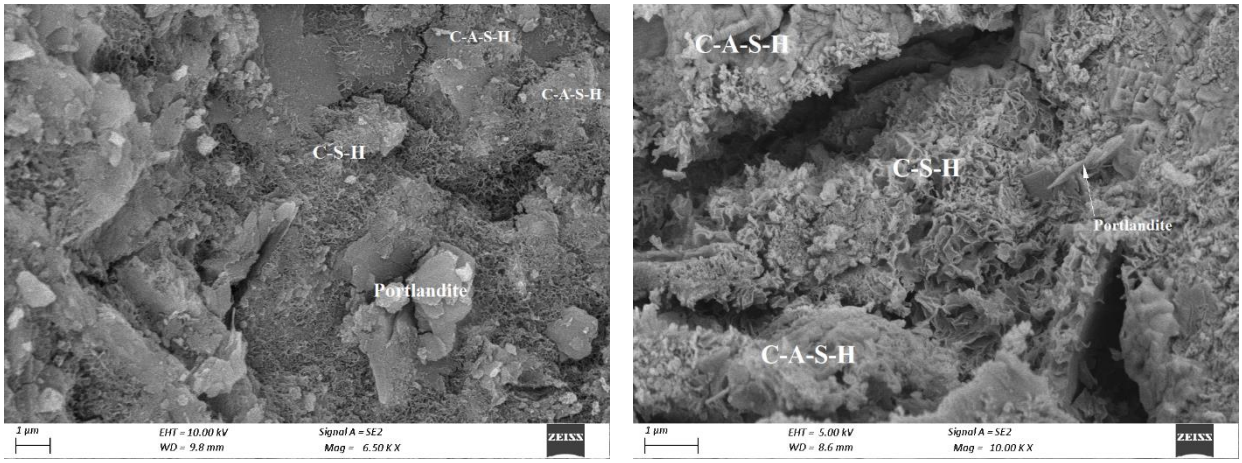

(a) (b)

Figure 6: SEM images of L20SF20 mortar containing 20% hydrated lime and 20% silica fume at (a) 7 days and (b) 28 days.

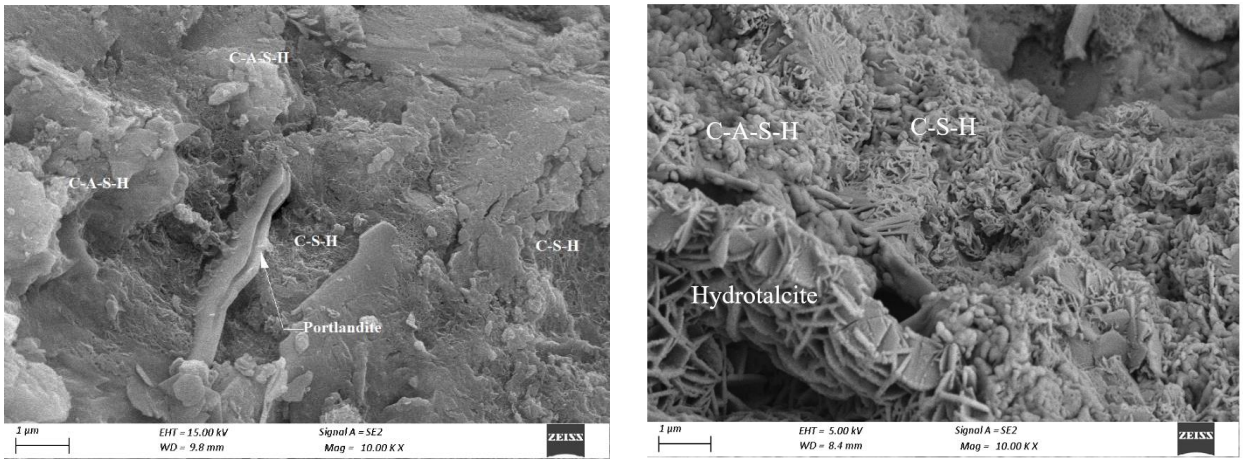

(a) (b)

Figure 7: SEM images of L30SF20 mortar containing 30% hydrated lime and 20% silica fume at (a) 7 days and (c) 28 days.

4. Conclusions

This study investigated the feasibility of utilizing hydrated lime as a solid activator for ground granulated blast furnace slag (GGBFS) activation, coupled with silica fume (SF) at varying percentages, up to 40%. Compressive strength demonstrated minimal variation, ranging from 20.53 to 27.16 MPa for SF variations of 10-30%. However, a notable 18-20% reduction in strength was observed at a 40% SF replacement. Optimal strength was achieved with SF replacement levels up to 30%, beyond which strength development was adversely impacted. In comparison to cement, the 7-day compressive strength reached a peak at 17.76 MPa, attributed to the initially lower pH upon water addition. To maintain a high system pH, a sodium-based activator is recommended. Primary hydration products included C-S-H and C-A-S-H, with the pozzolanic reaction surpassing the polymerization reaction. SEM analysis indicated that C-S-H governed the microstructural gel in the GGBFS and silica fume combination activated by hydrated lime. Future research aims to delve into microstructures in GGBFS and silica fume mixes activated by a combination of calcium and sodium-based activators, with an emphasis on ensuring simplicity and cost-effectiveness for the sodium-based activator.

Acknowledgment

The authors would like to thank the Structural Engineering Laboratory at IIT Kharagpur and the Central Research Facility at IIT Kharagpur for their assistance with the experiments.

References

[1] S. Louati, S. Baklouti, and B. Samet, "Geopolymers Based on Phosphoric Acid and Illito-Kaolinitic Clay," *Advances in Materials Science and Engineering*, vol. 2016, 2016, doi: 10.1155/2016/2359759.

[2] S. Louati, S. Baklouti, and B. Samet, "Acid based geopolymerization kinetics: Effect of clay particle size," *Appl Clay Sci*, vol. 132–133, 2016, doi: 10.1016/j.clay.2016.08.007.

[3] Y. He, L. Liu, L. He, and X. Cui, "Characterization of chemosynthetic H3PO4-Al2O3-2SiO2 geopolymers," *Ceram Int*, vol. 42, no. 9, 2016, doi: 10.1016/j.ceramint.2016.03.224.

[4] L. P. Liu, X. M. Cui, Y. He, S. D. Liu, and S. Y. Gong, "The phase evolution of phosphoric acid-based geopolymers at elevated temperatures," *Mater Lett*, vol. 66, no. 1, 2012, doi: 10.1016/j.matlet.2011.08.043.

[5] L. Xu, F. Matalkah, P. Soroushian, N. Darsanasiri, S. Hamadneh, and W. Wu, "Effects of citric acid on the rheology, hydration and strength development of alkali aluminosilicate cement," *Advances in Cement Research*, vol. 30, no. 2, 2018, doi: 10.1680/jadcr.16.00151.

[6] R. Vallepu *et al.*, "Effect of synthesis pH on the preparation and properties of K-Al-bearing silicate gels from solution," *Journal of the Ceramic Society of Japan*, vol. 114, no. 1331, 2006, doi: 10.2109/jcersj.114.624.

[7] I. Garcia-Lodeiro, A. Palomo, A. Fernández-Jiménez, and D. E. MacPhee, “Compatibility studies between N-A-S-H and C-A-S-H gels. Study in the ternary diagram Na2O-CaO-Al2O3-SiO 2-H2O,” *Cement and Concrete Research*, vol. 41, no. 9. 2011. doi: 10.1016/j.cemconres.2011.05.006.

[8] C. K. Yip, G. C. Lukey, and J. S. J. Van Deventer, “The coexistence of geopolymeric gel and calcium silicate hydrate at the early stage of alkaline activation,” *Cem Concr Res*, vol. 35, no. 9, 2005, doi: 10.1016/j.cemconres.2004.10.042.

[9] W. K. W. Lee and J. S. J. Van Deventer, “The effect of ionic contaminants on the early-age properties of alkali-activated fly ash-based cements,” *Cem Concr Res*, vol. 32, no. 4, 2002, doi: 10.1016/S0008-8846(01)00724-4.

[10] P. Chindaprasirt, C. Jaturapitakkul, W. Chalee, and U. Rattanasak, “Comparative study on the characteristics of fly ash and bottom ash geopolymers,” *Waste Management*, vol. 29, no. 2, 2009, doi: 10.1016/j.wasman.2008.06.023.

[11] J. Peyne, J. Gautron, J. Doudeau, E. Joussein, and S. Rossignol, “Influence of calcium addition on calcined brick clay based geopolymers: A thermal and FTIR spectroscopy study,” *Constr Build Mater*, vol. 152, pp. 794–803, Oct. 2017, doi: 10.1016/j.conbuildmat.2017.07.047.

[12] D. Jeon, Y. Jun, Y. Jeong, and J. E. Oh, “Microstructural and strength improvements through the use of Na2CO3 in a cementless Ca(OH)2-activated Class F fly ash system,” *Cem Concr Res*, vol. 67, 2015, doi: 10.1016/j.cemconres.2014.10.001.

[13] F. Massazza, “Pozzolanic cements,” *Cem Concr Compos*, vol. 15, no. 4, 1993, doi: 10.1016/0958-9465(93)90023-3.

[14] E. Vejmelková, M. Keppert, P. Rovnaníková, Z. Keršner, and R. Černý, “Properties of lime composites containing a new type of pozzolana for the improvement of strength and durability,” *Compos B Eng*, vol. 43, no. 8, 2012, doi: 10.1016/j.compositesb.2011.11.053.

[15] M. D. Jackson *et al.*, “Phillipsite and Al-tobermorite mineral cements produced through low-temperature water-rock reactions in Roman marine concrete,” *American Mineralogist*, vol. 102, no. 7, 2017, doi: 10.2138/am-2017-5993CCBY.

[16] M. D. Jackson *et al.*, “Unlocking the secrets of Al-tobermorite in Roman seawater concrete,” *American Mineralogist*, vol. 98, no. 10, 2013, doi: 10.2138/am.2013.4484.

[17] J. Davidovits, “Geopolymers - Inorganic polymeric new materials,” *Journal of Thermal Analysis*, vol. 37, no. 8, 1991, doi: 10.1007/BF01912193.

[18] J. Davidovits, “Geopolymers and geopolymeric materials,” *Journal of Thermal Analysis*, vol. 35, no. 2, 1989, doi: 10.1007/BF01904446.

[19] V. Pavlík and M. Užáková, “Effect of curing conditions on the properties of lime, lime-metakaolin and lime-zeolite mortars,” *Constr Build Mater*, vol. 102, 2016, doi: 10.1016/j.conbuildmat.2015.10.128.

[20] M. Stefanidou, E. C. Tsardaka, and E. Pavlidou, “Influence of nano-silica and nano-alumina in lime-pozzolan and lime-metakaolin binders,” in *Materials Today: Proceedings*, 2017. doi: 10.1016/j.matpr.2017.07.020.

[21] M. Heikal, H. Eldidamony, H. El-Didamony, M. Heikal, K. A. Khalil, and A. El-Sanhory, “Pozzolanic activity of silica fume with lime,” *Journal of Basic and Environmental Sciences*, vol. 4, no. August, pp. 236–246, 2017, [Online]. Available: https://www.researchgate.net/publication/319130806

[22] J. M. Paris, J. G. Roessler, C. C. Ferraro, H. D. Deford, and T. G. Townsend, “A review of waste products utilized as supplements to Portland cement in concrete,” *Journal of Cleaner Production*, vol. 121. 2016. doi: 10.1016/j.jclepro.2016.02.013.

[23] C. Shi, A. F. Jiménez, and A. Palomo, “New cements for the 21st century: The pursuit of an alternative to Portland cement,” *Cement and Concrete Research*, vol. 41, no. 7. Elsevier Ltd, pp. 750–763, 2011. doi: 10.1016/j.cemconres.2011.03.016.

[24] K. H. Mo, U. J. Alengaram, M. Z. Jumaat, S. P. Yap, and S. C. Lee, “Green concrete partially comprised of farming waste residues: A review,” *Journal of Cleaner Production*, vol. 117. 2016. doi: 10.1016/j.jclepro.2016.01.022.

[25] E. Aprianti, P. Shafigh, S. Bahri, and J. N. Farahani, “Supplementary cementitious materials origin from agricultural wastes - A review,” *Construction and Building Materials*, vol. 74. 2015. doi: 10.1016/j.conbuildmat.2014.10.010.

[26] M. C. G. Juenger and R. Siddique, “Recent advances in understanding the role of supplementary cementitious materials in concrete,” *Cement and Concrete Research*, vol. 78. 2015. doi: 10.1016/j.cemconres.2015.03.018.

[27] T. Luukkonen, Z. Abdollahnejad, J. Yliniemi, P. Kinnunen, and M. Illikainen, “One-part alkali-activated materials: A review,” *Cement and Concrete Research*, vol. 103. Elsevier Ltd, pp. 21–34, Jan. 01, 2018. doi: 10.1016/j.cemconres.2017.10.001.

[28] N. Ye *et al.*, “Synthesis and strength optimization of one-part geopolymer based on red mud,” *Constr Build Mater*, vol. 111, 2016, doi: 10.1016/j.conbuildmat.2016.02.099.

[29] B. Zhang, K. J. D. MacKenzie, and I. W. M. Brown, “Crystalline phase formation in metakaolinite geopolymers activated with NaOH and sodium silicate,” *J Mater Sci*, vol. 44, no. 17, 2009, doi: 10.1007/s10853-009-3715-1.

[30] A. Hajimohammadi and J. S. J. van Deventer, “Solid Reactant-Based Geopolymers from Rice Hull Ash and Sodium Aluminate,” *Waste Biomass Valorization*, vol. 8, no. 6, 2017, doi: 10.1007/s12649-016-9735-6.

[31] Y. J. Patel and N. Shah, “Enhancement of the properties of Ground Granulated Blast Furnace Slag based Self Compacting Geopolymer Concrete by incorporating Rice Husk Ash,” *Constr Build Mater*, vol. 171, pp. 654–662, May 2018, doi: 10.1016/j.conbuildmat.2018.03.166.

[32] Y. Y. Kim, B. J. Lee, V. Saraswathy, and S. J. Kwon, “Strength and durability performance of alkali-activated rice husk ash geopolymer mortar,” *Scientific World Journal*, vol. 2014, 2014, doi: 10.1155/2014/209584.

[33] B. Adeleke, J. Kinuthia, and J. Oti, “Optimization of MgO-GGBS cementitious systems using thermo-chemical approaches,” *Sustainability (Switzerland)*, vol. 13, no. 16, 2021, doi: 10.3390/su13169378.

[34] M. Ben Haha, B. Lothenbach, G. Le Saout, and F. Winnefeld, “Influence of slag chemistry on the hydration of alkali-activated blast-furnace slag - Part I: Effect of MgO,” *Cem Concr Res*, vol. 41, no. 9, 2011, doi: 10.1016/j.cemconres.2011.05.002.